

## Fracture pattern of stainless Cr-Mn-N steel with nanostructured surface layers at cryogenic temperature

© N.A. Narkevich,<sup>1</sup> I.V. Vlasov,<sup>1</sup> Yu.F. Gomorova,<sup>1</sup> M.S. Syrtanov,<sup>2</sup> A.I. Tolmachev,<sup>1</sup> M.N. Volochaev<sup>3</sup>

<sup>1</sup> Institute of Strength Physics and Materials Science, Siberian Branch, Russian Academy of Sciences, 634055 Tomsk, Russia

<sup>2</sup> Tomsk Polytechnic University, 634050 Tomsk, Russia

<sup>3</sup> Kirensky Institute of Physics, Federal Research Center KSC SB, Russian Academy of Sciences, 660036 Krasnoyarsk, Russia  
e-mail: natnark@list.ru

Received April 18, 2023

Revised September 26, 2023

Accepted November 10, 2023

Effect of deformation treatment of the surface of stainless austenitic Cr-Mn-N steel on its structure, mechanical properties and fracture behavior at  $-196^{\circ}\text{C}$  has been studied. Structure refinement, decrease in the lattice parameter of austenite and strain aging with the formation of CrN and Fe<sub>2</sub>N particles occurs during processing in the near-surface layer. After processing, the steel has an increased yield strength and work hardening, but reduced ductility and toughness compared to the quenched state. Dimple fracture of near-surface layers is facilitated by a decrease in internal stresses associated with the release of nitrogen from interstitial positions and the formation of nitrides.

**Keywords:** high nitrogen steel, austenite, ultrasonic forging strain, nanostructure, tension, impact bending, plasticity, fracture toughness, fracture.

DOI: 10.61011/JTF.2024.01.56906.96-23

### Introduction

Nickel-free high-nitrogen austenitic steels at climatic temperatures can be used as an alternative to Cr-Ni steels because of their combination of their low cost with higher strength, ductility and corrosion resistance [1,2]. They can be utilized in building structures [3,4] and offshore platforms [5] operating in the high latitudes of the Far North, in the Arctic areas. The application of this class of steels in systems used for the production, transportation and storage of liquefied natural gas at cryogenic temperatures is hindered by a pronounced visco-brittle transition observed both under static tension and impact bending [6–14].

The efforts made to improve the fracture toughness of high-nitrogen steels are mainly aimed at optimizing the alloying system. In particular, additional alloying with copper contributed to an increase of the toughness of Cr-Mn-N steels [7], and both ductility and toughness are improved with an increase of Mn content at low temperatures [8]. The introduction of Ni and Cu stabilized austenite and thereby lowered the temperature of the visco-brittle transition [10]. C+N alloyed steels had a lower visco-brittle transition temperature in comparison with steels alloyed only with nitrogen owing to the increased metallic nature of the interatomic bond [11]. The solution for overcoming the brittle fracturing and increasing the impact strength have not yet been developed despite the need for nickel-free stainless steels for use not only at low climatic temperatures, but also at cryogenic temperatures. The contemporary views attribute the brittleness of high-

nitrogen steels at low and cryogenic temperatures to a higher activation energy for dislocation glide [6], a decrease of the stacking fault energy (SFE) and activation of planar sliding along planes  $\{111\}$  with a high density of dislocations [9,12], stabilization of austenite and the absence of martensitic  $\gamma \rightarrow \alpha'$ -transformations as an effective mechanism for suppressing the nucleation and growth of cracks [15], the hardening effect of nitrogen and high yield strength [16].

The improvement of crack resistance and impact strength, as well as the improvement of other physical and mechanical properties of metals and alloys is facilitated by grinding their structure to a nanoparticle size [17–20]. The grinding of the structure by deformation of high-nitrogen steels has a positive effect on the strength properties [21–25]. Phase transformations are observed [21,22], strain aging takes place [23,24] due to local strain heating in the case of surface strain hardening in near-surface layers. At the same time the strain-induced dissolution of nitrides is observed in case of shearing stain under pressure at room temperature or at the liquid nitrogen temperature without strain heating [26–28]. The structure formed in the process of intense deformation largely depends on local thermal fluctuations and the character of the stress condition. The formation of  $\epsilon$ -martensite with a HCP lattice with a smaller crystal lattice volume than austenite is possible in the regions of local compression [26], while the release of CrN nitrides with a large volume of the crystal lattice is possible in the regions of local extension [23].

This study investigates the impact of structural changes in high-nitrogen Cr-Mn-N steel in case of severe plastic strain on the strain behavior and the nature of failure at  $-196^{\circ}\text{C}$ .

## 1. Material and research techniques

The studied steel was smelted in an induction furnace with a chromium-magnesite lining. Armco-iron, low-carbon ferrochrome, metallic manganese, and nitrated ferrochrome were used as a charge. The molten metal was first poured into a ladle from the furnace, then it was poured into 5 sand molds. The chemical composition of the investigated Cr-Mn-N-steel is provided in the table.

Chemical composition of steel

Element	Cr	Mn	Si	Ni	C	N	P	S	Fe
Weight, %	16.50	18.81	0.52	0.24	0.07	0.53	0.01	0.001	Bal.

The ingots were forged and cut into 10 mm thick, 20 mm wide and 100 mm long plates. The steel had a single-phase large-crystal austenitic structure with a grain size of  $30\text{--}50\mu\text{m}$  after tempering of the plates from  $1100^{\circ}\text{C}$  in water. One of the surfaces of the steel plates was sanded and polished with diamond pastes. After that, hardening strain treatment was carried out by forging with strikers with ultrasonic frequency followed by ultrasonic forging.

The surface ultrasonic forging was performed at room temperature in air with a forging tool using an ultrasonic generator UZG 06/27 (output power 550 W, generator frequency 25 kHz, transducer amplitude  $15\mu\text{m}$ ). Three asynchronously operating axially moving impactors (forging tool parts) were applied to the treated surface with a load of 70 N. The impactors were loaded and moved in vertical plane by a spring, which is part of the forging tool. The treated surface moved with a speed of 20 mm/s relative to the forging tool.

Tensile test specimens with a working length of 15 mm and cross-sectional dimensions of  $1 \times 2.5\text{ mm}$  were cut from the plate using an electric spark method, as shown in Fig. 1, *a*. The second, untreated surface was sanded and polished with diamond pastes.

Other samples were prepared for impact bending tests. The surfaces of the hardened plate with a width of 20 mm and a length of 100 mm were ground and polished, and then they were treated by ultrasonic forging. 10 mm thick, 5 mm wide and 55 mm long standard Charpy V-notched samples were cut from this plate using an electrospark discharge machine (Fig. 1, *b*). The side faces of the prepared samples were treated by ultrasonic forging.

Tensile testing of the samples was performed using testing machine (Instron 5582, Norwood, MA, USA) at a temperature of  $-196^{\circ}\text{C}$  with a deformation rate of  $1.33 \cdot 10^{-4}\text{ s}^{-1}$ . Samples after tempering were used for comparison under the same conditions. The surfaces of the hardened samples were ground and polished using diamond

pastes prior to tensile and impact bending tests. 3 samples were tested in each case.

Testing was performed using Instron 450MPX testing machine (Grove City, PA USA) with the impact velocity of 5.3 m/s. The samples were pre-cooled in liquid nitrogen to  $-196^{\circ}\text{C}$ . The time interval during which the samples were moved from the thermostat with liquid nitrogen to the testing machine and tested did not exceed 5 s. Samples after tempering were used for comparison under the same conditions. At least 3 samples were tested in each case.

Transmission electron microscope (TEM) (Hitachi HT-7700, Japan) with an accelerating voltage of 120 kV was used to study structure of the steel surface layer after ultrasonic forging. The cross sections were made using a system of focused ion beam FB-2100 (Hitachi, Japan).

X-ray diffractometry was used to study the steel crystal structure with diffractometer XRD-7000 (Shimadzu, Japan) in  $\text{CuK}\alpha$  radiation at room temperature. The Williamson-Hall [29] method was used to determine the main parameters of the crystal structure, such as the size of coherent scattering regions (CSR), intragrain microdeformations  $\langle\epsilon\rangle$ .

The fracture surfaces were studied using a scanning electron microscope LEO EVO,50 (Zeiss, Germany).

## 2. Study results and their discussion

### 2.1. Structure study

The thickness of the deformed layer after ultrasonic forging is of the order of  $150\text{--}200\mu\text{m}$  according to metallographic analysis [23]. No changes of the phase composition were found by X-ray diffraction analysis of this layer of austenitic steel in comparison with the post-tempering condition (Fig. 2, *a*). A decrease of the austenite lattice parameter is one of the treatment effects (Fig. 2, *b*). Another effect is the dispersion of the structure to a nanoparticle level with  $D = 18\text{ nm}$  CSR and  $\langle\epsilon\rangle = 0.17\%$  of FCC lattice microdeformations.

Fig. 3 shows the TEM image of the structure. The ring electron diffraction pattern corresponds to highly dispersed austenitic structure with continuous and discrete misorientation of its fragments (Fig. 3, *b*). The size of the fragments of the structure in the dark-field image (Fig. 3, *c*) does not exceed 30 nm. Apart from rings, the electron diffraction pattern also includes reflexes of other phases with interplanar distances different from those present in austenite. Some of them form reflex nets. Fig. 3, *b* shows one of the nets with the zone axis  $[11\bar{2}]$ . The phase was identified as CrN nitride ( $d_{(111)} = 0.240\text{ nm}$ ,  $d_{(220)} = 0.146\text{ nm}$ ) with a FCC lattice based on the interplane distances and the angle between the directions. Bright nitrides with size of 1–3 nm are seen in the dark-field image of the structure in the reflex  $(11\bar{1})_{\text{CrN}}$  (Fig. 3, *d*). There are also areas with the size of up to 10 nm. The other net is formed by reflexes related to the axis of the zone  $[001]_{\text{CrN}}$  (Fig. 3, *b*) which separately accommodates reflex  $(\bar{2}\bar{2}0)_{\text{CrN}}$  and reflexes of

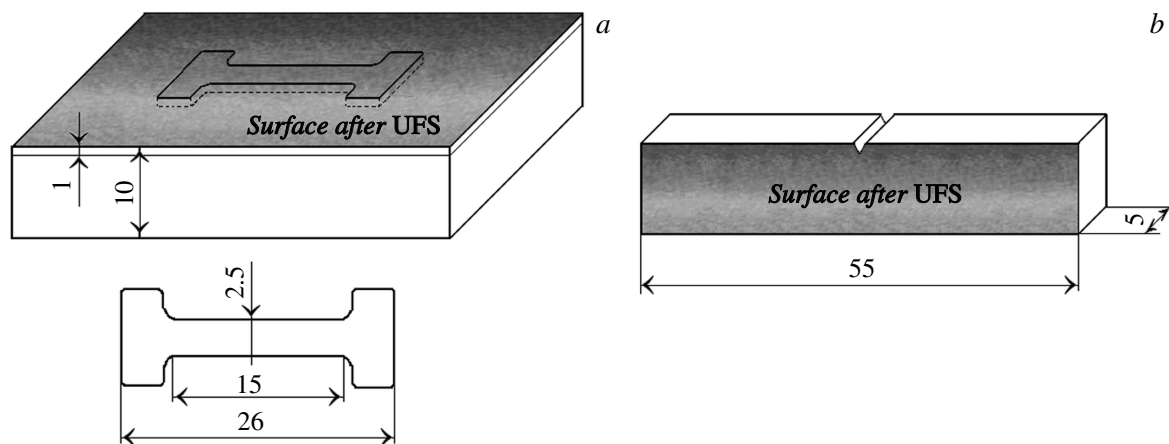


**Figure 1.** Cutting pattern and sample sizes in millimeters for static tensile tests (a) and impact bending (b).

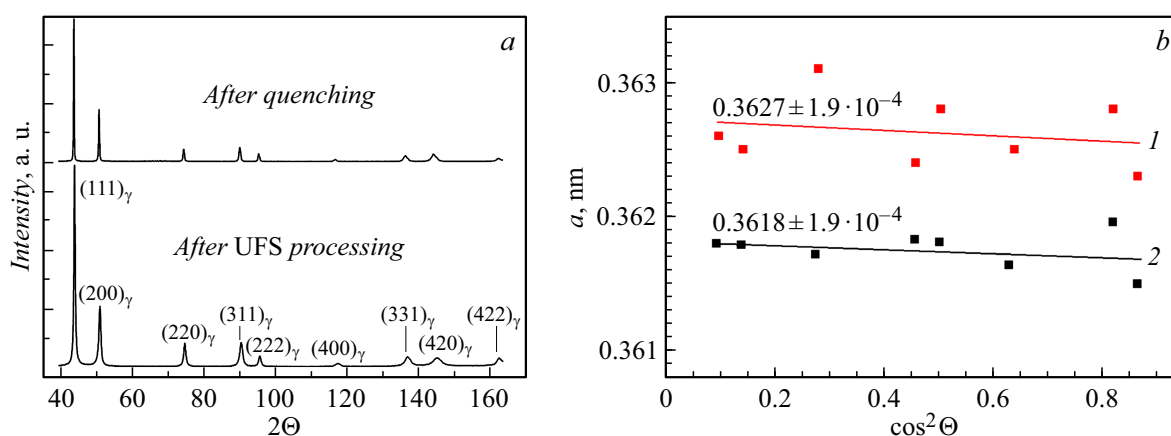


**Figure 2.** a — diffractograms of Cr-Mn-N steel after tempering and tempering followed ultrasonic forging; b — parameters of the austenite lattice after tempering (1) and tempering followed ultrasonic forging (2).

$\{200\}_{\text{CrN}}$  type are located on the ring  $\{111\}_\gamma$ , because the corresponding crystallographic planes of nitride and austenite have close interplane distances ( $d_{(111)\gamma} = 0.208$  nm;  $d_{(200)\text{CrN}} = 0.207$  nm).

A net of reflexes of another nitride  $\text{Fe}_2\text{N}$  with an orthorhombic lattice, parameters  $a=0.6147$ ,  $b=0.5034$ ,  $c=0.4367$  nm and interplanar spacing  $d_{(121)} = 0.2055$ ,  $d_{(002)} = 0.2183$ ,  $d_{(\bar{2}40)} = 0.1165$  nm, first discovered by us in [23] is shown on the electron diffraction pattern (Fig. 3, b). The formation of  $\text{Fe}_2\text{N}$  during the aging of high-nitrogen steels was not observed before, since the interaction of chromium and nitrogen producing  $\text{Cr}_2\text{N}$  nitride is thermodynamically more advantageous. According to the formation of CrN and  $\text{Fe}_2\text{N}$  nitrides in the conditions of low diffusion mobility of atoms and high local tensile stresses is associated with the type of their crystal lattices, which ensures the best coupling of the matrix and secondary phases.

Therefore, the analysis of TEM images of the structure showed that strain aging occurs in the dispersed austenitic structure of the near-surface layer during strain treatment

at room temperature. The formation of CrN and  $\text{Fe}_2\text{N}$  nitrides in the result of cold strain treatment by ultrasonic forging indicates, firstly, a strongly nonequilibrium state of a solid solution doped with nitrogen, and, secondly, that strain aging in this case is a mechanism of relaxation of internal stresses caused by doping. The relaxation process is evidenced by a decrease of the lattice constants and the fact that the lattice volumes of CrN and  $\text{Fe}_2\text{N}$  nitrides are larger than the lattice volume of the matrix phase, therefore, they are formed in local areas of tensile stresses.

## 2.2. Tensile tests

It is well known [18] that in the limited deformed state the metal materials have low plasticity. The plasticity becomes even lower at negative deformation temperatures. The properties of high-nitrogen steel at cryogenic temperature with and without a hardened surface layer can be judged by Fig. 4, which characterizes the typical strain behavior and properties for each series of samples.

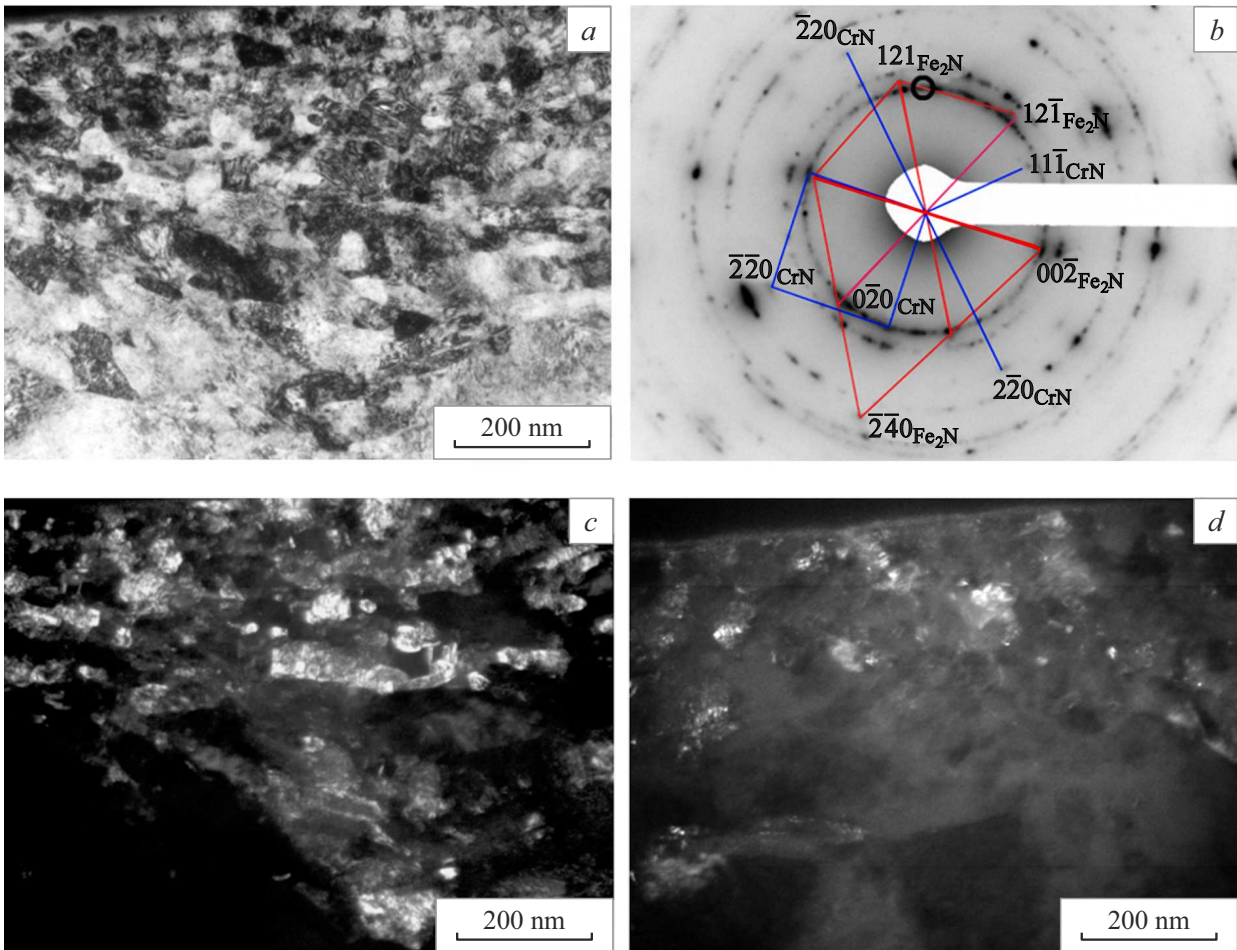


**Figure 3.** The structure of the near-surface layer of Cr-Mn-N-steel after ultrasonic forging: *a* — bright field image; *b* — electron diffraction pattern with CrN reflex grids  $z = [112]_{\text{CrN}}$  and  $[001]_{\text{CrN}}$ , as well as a grid of reflexes  $\text{Fe}_2\text{N}$   $z = [2\bar{1}0]_{\text{Fe}_2\text{N}}$ ; *c* — dark-field image in a fragment of a ring highlighted by a selector diaphragm on the electron diffraction pattern; *d* — dark-field image in reflex  $(11\bar{1})_{\text{CrN}}$ .

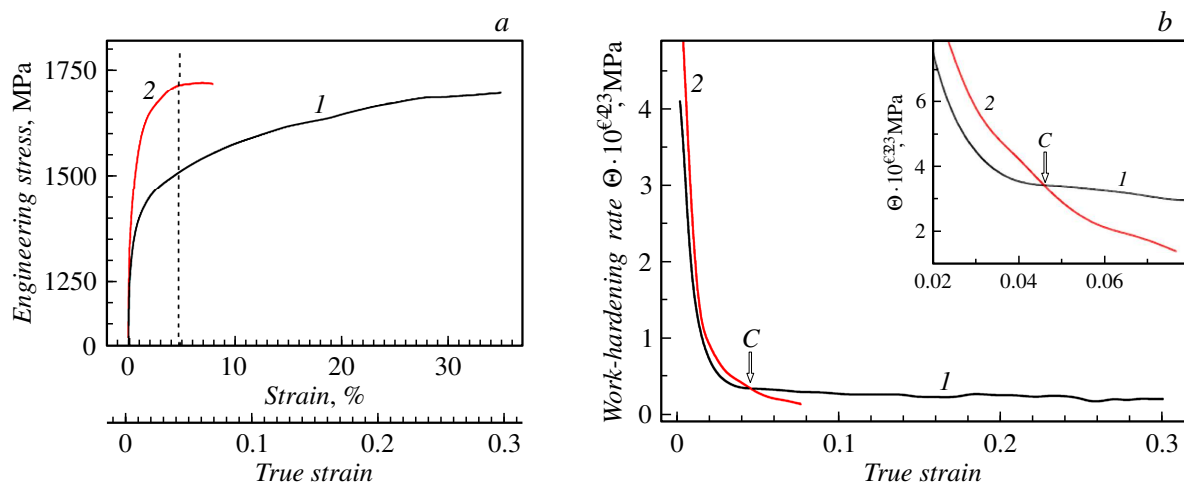


**Figure 4.** Curves  $\delta$ – $\varepsilon$  (*a*) and the change of the strain hardening rate (*b*) in case of tensile testing of Cr-Mn-N-steel at  $-196^\circ\text{C}$  after tempering from  $1100^\circ\text{C}$  (*1*) and after ultrasonic forging (*2*).

It is apparent that ultrasonic forge treatment increases the yield strength, but does not affect the tensile strength.

Obviously, the increase of yield strength is attributable to the high resistance to strain of the near-surface layer with a

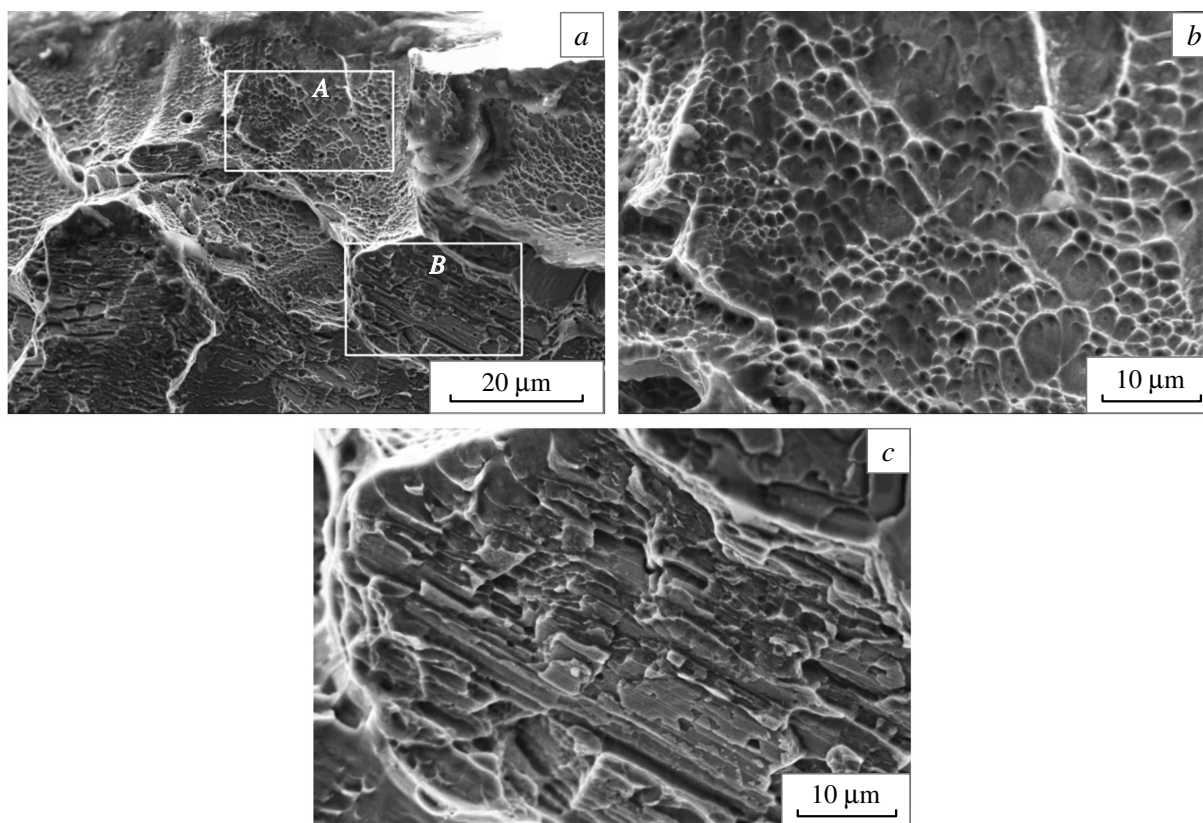


**Figure 5.** Cr-Mn-N-steel fracture topography with a surface treated by ultrasonic forging and subjected to tensile testing at  $-196^{\circ}\text{C}$  (*a*); enlarged image of the fragment A (*b*), enlarged image of the fragment B (*c*).

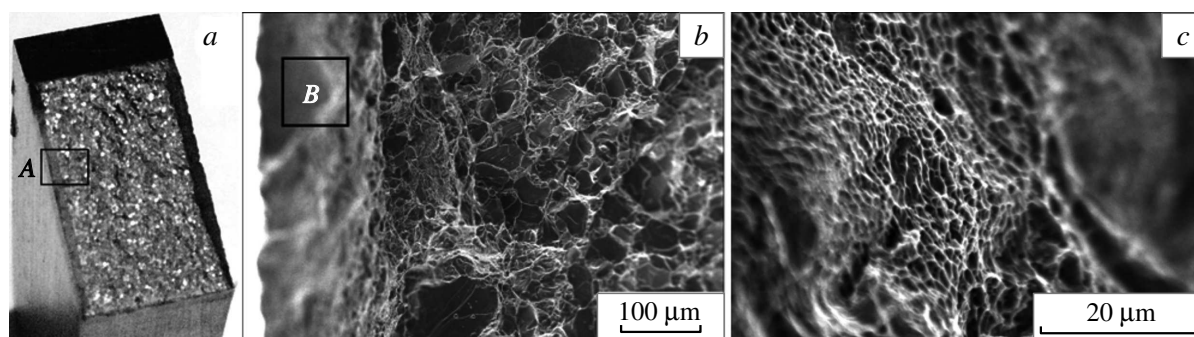


**Figure 6.** Fracture topography of hardened Cr-Mn-N steel after impact bending tests at  $-196^{\circ}\text{C}$ : macrorelief (*a*); microrelief of the fragment A (*b*); microrelief of the lips of the fragment section B (*c*).

nanostructure, and the strength value is determined by the structure in the central part of the sample. The moment when this layer stops to perform the function of a barrier for tensile plastic strain because of its failure corresponds to strain  $\varepsilon_{\text{true}} = 0.046$  at the point C in Fig. 4, *b*. The strain hardening rate of the sample becomes less than the corresponding characteristic of the untreated sample to the right of this point.

The work of plastic strain, defined by the area bounded by the curve 2 in Fig. 2, *a*, before strain  $\varepsilon_{\text{true}} = 0.046$  by 13% more than the corresponding value for the curve 1,

which indicates a limitation of the structural mechanisms of relaxation of external stresses in the nanostructured layer. Therefore, the experimental results indicate that the surface treatment of the studied steel reduces its ductility, but the plasticity of the nanostructured layer is quite high,  $\sim 5\%$  at the same time.

The study of the topography of the surface of the destroyed samples revealed a difference in the micromechanisms of destruction of the near-surface nanodisperse layer containing particles CrN and Fe<sub>2</sub>N and the rest of the sample section (Fig. 5).

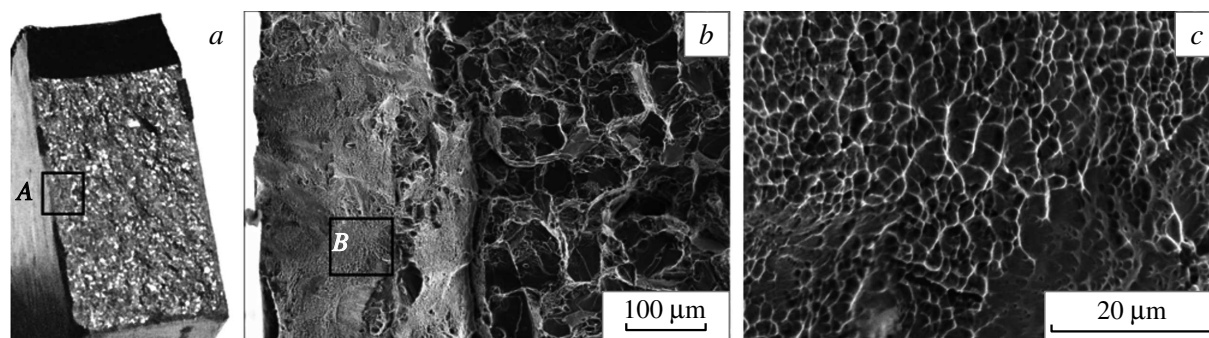


**Figure 7.** The topography of fracture of the tempered Cr-Mn-N-steel which is then treated by ultrasonic forging after impact bending testing at  $-196^{\circ}\text{C}$ : *a* — macrorelief; *b* — microrelief of the fragment A; *c* — microrelief of the near-surface layer of the fragment B.

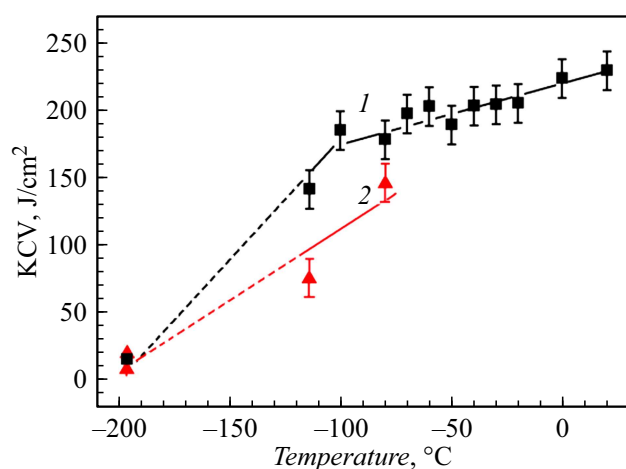


**Figure 8.** The dependence of KCV on the test temperature of Cr-Mn-N-steel after tempering 1 — from  $1100^{\circ}\text{C}$  [30] and 2 — after ultrasonic forging

The near-surface layer with a dispersed structure in high-nitrogen austenitic Cr-Mn-N steel shows a ductile failure in case of subsequent deformation at  $-196^{\circ}\text{C}$ . The structure refinement to a nanoscale level reduces the mobility of dislocations, the length of their free path, and prevents the occurrence of martensitic transformations.

The remaining part of the sample shows a brittle failure. The fracture has a specific lamellar structure. The failure of this type is attributable to  $\epsilon$ -martensite with a HCP lattice [30,31] as a result of the TRIP effect caused by the dislocation mechanism [32].

### 2.3. Impact bending tests

Our previous study [31] showed a ductile failure of tempered steel in the temperature range from  $-114$  to  $+20^{\circ}\text{C}$  forming a dimpled microrelief. Brittle transcrystalline fracture by chipping is a dominant mechanism of sample failure in the central part at  $-196^{\circ}\text{C}$ . There is great freedom for the development of the plastic flow of the material near free surfaces [33], a plane stress state occurs [34]. Shear lips

are formed under the action of maximum tangential stresses at an angle of  $45^{\circ}$  with a dimpled relief characteristic of a ductile micromechanism of destruction are formed (Fig. 6). A transition zone with a mixed brittle and ductile micromechanism of destruction can be defined.

Strain treatment by ultrasonic forging prevents plastic flow near the lateral faces of the samples and thereby affects the nature of the stress state in these zones with a change to a close to plain strain. This is evidenced by the absence of shear lips near the free surfaces treated by ultrasonic forging and absence of tightening near the fracture (Fig. 7, *a*). The testing of steel of similar composition for static crack resistance at  $-196^{\circ}\text{C}$  provided a similar result [34]. Nevertheless, (Fig. 7, *b, c*) shows that the micromechanism of failure of subsurface layers hardened by ultrasonic forging is ductile. A dimpled fracture with equiaxed pits indicates normal separation stresses. The thickness of the near-surface ductile fractured layer is greater than its thickness at the lips of the section of tempered steel, and varies within  $200\text{--}300\ \mu\text{m}$ . A distinct gradient is visible on the topographic image of the fracture in the absence of a transition layer with a mixed type of fracture (Fig. 7, *b*).

At the same time, nanostructuring of the surface layers did not increase the energy intensity of steel destruction, which manifested itself in a decrease of its toughness. A reduction of the impact strength of KCV was also recorded at other temperatures —  $-100$  and  $-80^{\circ}\text{C}$  (Fig. 8).

A comparison of the impact loading curves at temperatures  $-110$  and  $-80^{\circ}\text{C}$  of samples without strain treatment and after ultrasonic treatment showed that strain treatment contributes to an increase of strain hardening (angle of inclination of the ascending branch) and maximum load by  $\Delta F$  at the stage of plastic yield and nucleation of the main fracture (Fig. 9). At the same time, the ultrasonic forging impact on the work of plastic deformation and crack nucleation (the area under the ascending branch) is insignificant and increases in some samples and decreases in other samples. The ultrasonic forging has the most significant impact on the stage of fracture propagation, which starts at the moment of a steady decrease of the load in case of impact bending. A decrease of the crack

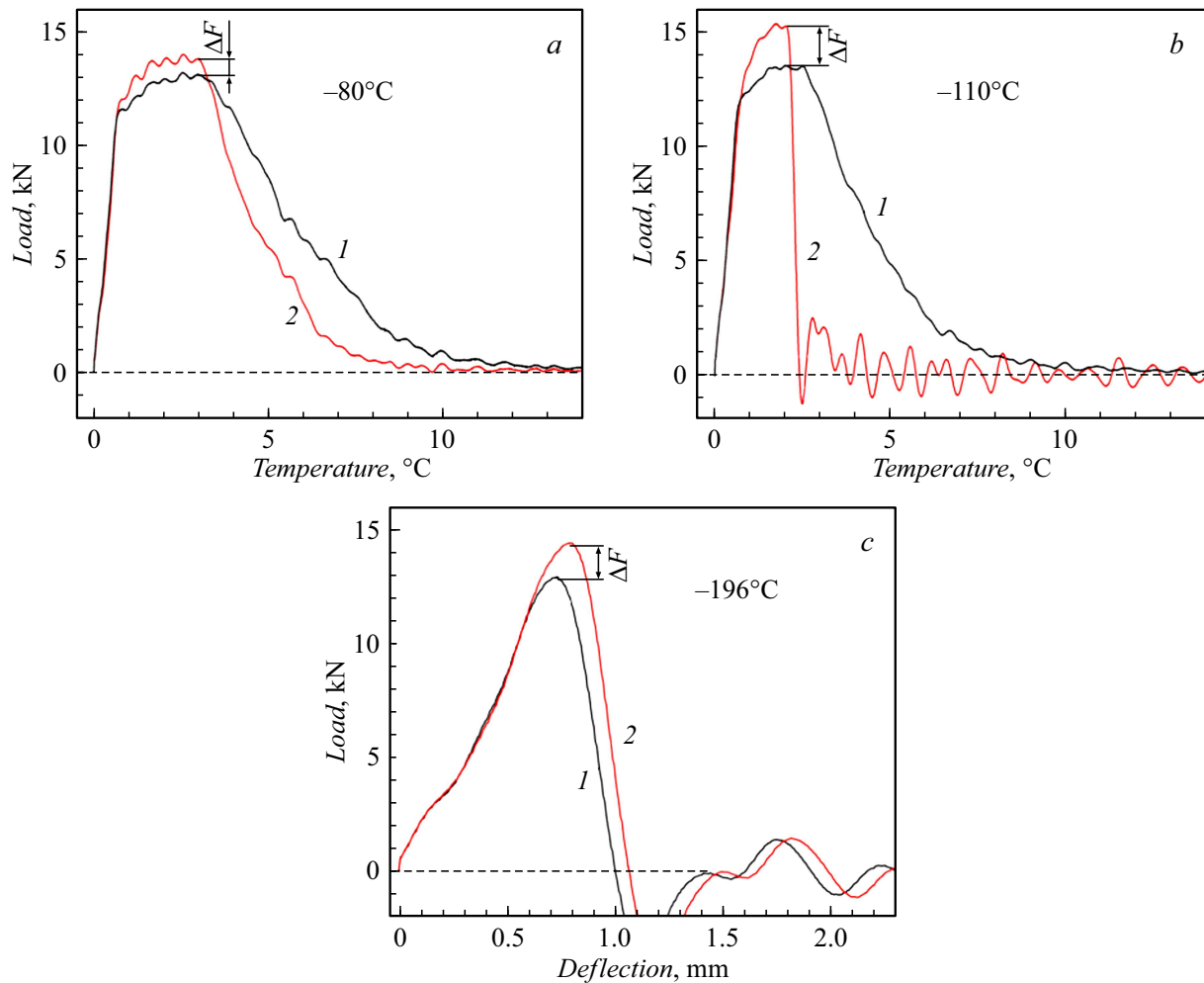


**Figure 9.** Impact loading curves of Cr-Mn-N-steel at  $-80$  (a),  $-110$  (b),  $-196^{\circ}\text{C}$  (c) after tempering from  $1100^{\circ}\text{C}$  (1) and after ultrasonic forging (2).

propagation work (the area under the descending branch of the curve) indicates a low dynamic crack resistance of steel [35] treated by ultrasonic forging at all temperatures studied. Other materials with FCC, BCC and HCP nanodisperse structure [35] also have low dynamic crack resistance.

The energy intensity of the nucleation of the main crack and its propagation at cryogenic temperature is extremely low in both cases (Fig. 9, c).

In our opinion, the brittle transcrystalline fracture by chipping and quasi-chipping of high-nitrogen steels is attributable to the highly stressed state formed at cryogenic temperature because of a decrease of the volume of the FCC lattice, with a constant concentration and radius of nitrogen atoms embedded in the lattice. Internal stresses increase as the test temperature decreases and reach critical values at  $-196^{\circ}\text{C}$ . Stress relaxation under impact loading occurs without significant inclusion of dislocation mechanisms of plastic deformation.

A ductile pit fracture of the near-surface layer, both under tension and under impact bending at cryogenic temperature, is formed due to a local decrease of internal stresses in this layer because of the release of nitrogen from the insertion positions and the formation of nitrides in the ultrasonic forging process. This conclusion is consistent with data on an increase of the temperature of the ductile and brittle transition with an increase of the concentration of dissolved nitrogen [6]. Along with the presence of a clear sign of the ductility of steel in the form of a pit fracture, there are also obvious signs of brittleness in the near-surface layers treated with ultrasonic forging: the absence of tightening on the side faces of the Charpy samples and the shear lips the almost complete absence of a plastic deformation area on the impact bending diagram. The structure atomization by intensive strain to an extremely high degree forms a highly defective structure in which dislocation slip is complicated. The steel hardening by surface strain treatment prevents the relaxation process during the testing process. Therefore, the plasticity and impact strength decrease despite the formation of a pit fracture in part of the section.

## Conclusion

The studies of the structure and nature of destruction at cryogenic temperature of high-nitrogen stainless Cr-Mn-N steel, the structure of the surface layers of which is refined by intensive deformation to the nanoscale level, showed the following.

1. The strain aging with the formation of nitrides CrN and Fe<sub>2</sub>N during intensive strain (ultrasonic forging) of near-surface layers is accompanied by a decrease of the parameter of the austenite lattice and indicates a decrease of internal stresses.

2. Preliminary ultrasonic forging suppresses martensitic transformations under static tension, contributes to an increase of the strain hardening, yield strength, does not affect the ultimate strength and reduces ductility.

3. The impact strength of steel with surface layers hardened by ultrasonic forging, is lower than after tempering from 1100°C.

4. The surface layers treated by ultrasonic forging show ductile fracturing with the formation of a dimpled relief. The ductile failure micromechanism is attributable to the strain aging, which contributes to a decrease of internal stresses in the FCC lattice because of the release of nitrogen from the nitride injection and formation positions.

## Acknowledgments

Structural research was carried out using the equipment provided by the Krasnoyarsk Regional Center for Collective Use, Federal Research Center, Krasnoyarsk Scientific Center of the Siberian Branch of the Russian Academy of Sciences. Fractographic studies were performed using the equipment of common use center „Nanotech“ of ISPMS SB RAS“.

## Funding

This study was supported financially by the Russian Science Foundation (grant № 22-29-00438).

## Conflict of interest

The authors declare that they have no conflict of interest.

## References

- [1] V.V. Sagaradze, A.I. Uvarov. *Uprochnenie i svoystva austenitnykh stalej* (Editorial and Publications Division of Ural Branch of Russian Academy of Sciences, Yekaterinburg, 2013) (in Russian).
- [2] V.G. Gavriljuk, H. Berns. *High Nitrogen steels — Structure, Properties, Applications* (Springer, Berlin, 1999)
- [3] J.-B. Yan, Y. Geng, P. Xie, J. Xie. *Constr. Build. Mater.*, **343**, 128122 (2022). DOI: 10.1016/j.conbuildmat.2022.128122
- [4] N.R. Baddoo. *J. Constr. Steel Res.*, **64**(11), 1199 (2008). DOI: 10.1016/j.jcsr.2008.07.011
- [5] P. Layus, P. Kah, J. Martikainen, M. Pirinen, E. Khlushova, A. Ilyin. In *Proceed. XXIII Int. Conf. Offshore and Polar Engineering* (Anchorage, 2013), p. 242. <https://www.researchgate.net/publication/267450237>
- [6] M. Tanaka, T. Onomoto, T. Tsuchiyama, K. Higashida. *ISIJ Int.*, **52**(5), 915 (2012). DOI: 10.2355/isijinternational.52.915
- [7] M. Milititsky, D.K. Matlock, A. Regully, N. Dewispelaere, J. Penning, H. Hanninen. *Mater. Sci. Eng.: A*, **496**, 189 (2008). DOI: 10.1016/j.msea.2008.05.022
- [8] M. Xu, J. Wang, C. Liu. *Acta Metall. Sin.*, **47**(10), 1335 (2011). DOI: 10.3724/SP.J.1037.2011.00141
- [9] Y. Tomota, Y. Xia, K. Inoue. *Acta Mater.*, **46**(5), 1577 (1998). DOI: 10.1016/S1359-6454(97)00350-9
- [10] B. Hwang, T.-H. Lee, S.-J. Park, Ch.-S. Oh, S.-J. Kim. *Mater. Sci. Forum*, **654–656**, 158 (2010). DOI: 10.4028/www.scientific.net/MSF.654-656.158
- [11] B. Hwang, T.-H. Lee, S.-J. Kim. *Proceed. Eng.*, **10**, 409 (2011). DOI: 10.1016/j.proeng.2011.04.069
- [12] Y. Tomota, J. Nakano, Y. Xia, K. Inoue. *Acta Mater.*, **46**(9), 3099 (1998). DOI: 10.1016/s1359-6454(98)00005-6
- [13] G. Sun, Yu. Zhang, S. Sun, J. Hu, Z. Jiang, C. Ji. *Mater. Sci. Eng.: A*, **662**, 432 (2016). DOI: 10.1016/j.msea.2016.03.057
- [14] G. Sun, A. Yu, S. Sun, C. Ji, J. Hu, Z. Jiang, J. Lian. *Mater. Sci. Tech.*, **33**(14), 1635 (2017). DOI: 10.1080/02670836.2017.1306012
- [15] S. Wang, K. Yang, Y. Shan, L. Li. *Mater. Sci. Eng.: A*, **490**, 95 (2008). DOI: 10.1016/j.msea.2008.01.015
- [16] R.J. Ilola, H.E. Hänninen, K.M. Ullakko. *ISIJ Int.*, **36**(7), 873 (1996). DOI: 10.2355/isijinternational.36.873
- [17] Yu.R. Kolobov, S.S. Manokhin, V.I. Betekhtin, A.G. Kadomtsev, M.V. Narykova, G.V. Odintsova, G.V. Khramov. *Tech. Phys. Lett.*, **48**(1), 56 (2022). DOI: 10.21883/TPL.2022.01.52471.19025
- [18] R.Z. Valiev, Yu. Estrin, Z. Horita, T.G. Langdon, M.J. Zechetbauer, Yu.T. Zhu. *JOM*, **58**(4), 33 (2006). DOI: 10.1007/s11837-006-0213-7
- [19] J.W. Bae, P. Asghari-Rad, A. Amanov, H.S. Kim, *Mater. Sci. Eng.: A*, **826**, 141966 (2021). DOI: 10.1016/j.msea.2021.141966
- [20] G.V. Klevtsov, N.A. Klevtsova, R.Z. Valiev, I.N. Pigaleva, O.A. Frolova. *Vestnik Tambovskogo un-ta. Seriya Estestvennyye i tekhnicheskie nauki*, **21**(3), 772 (2016) (in Russian). DOI: 10.20310/1810-0198-2016-21-3-772-775
- [21] V.V. Sagaradze, N.V. Kataeva, I.G. Kabanova, S.V. Afanasev, A.V. Pavlenko. *Phys. Met. Metallogr.*, **121**(7), 683 (2020). DOI: 10.1134/S0031918X20070091
- [22] N.A. Narkevich, A.I. Tolmachev, I.V. Vlasov, N.S. Surikova. *Phys. Met. Metallogr.*, **117**(3), 298 (2016). DOI: 10.1134/S0031918X16030108
- [23] N.A. Narkevich, E.E. Deryugin, O.B. Perevalova, I.V. Vlasov. *Mater. Sci. Eng.: A*, **834**, 142590 (2022). DOI: 10.1016/j.msea.2021.142590
- [24] N.A. Narkevich, E.E. Deryugin, I.V. Vlasov. *Tech. Phys. Lett.*, **48**(5), 13 (2022). DOI: 10.21883/TPL.2022.05.53469.19145
- [25] N.A. Narkevich, M.N. Volochaev, I.A. Shulepov, Yu.F. Gomorova. *Phys. Met. Metallogr.*, **123**(10), 1024 (2022). DOI: 10.1134/S0031918X22601007
- [26] V. Shabashov, K. Lyashkov, K. Kozlov, V. Zavalishin, A. Zamatovskii, N. Kataeva, V. Sagaradze, Yu. Ustyugov. *Materials*, **14**, 7116 (2021). DOI: 10.3390/ma14237116

- [27] A.V. Makarov, S.N. Luchko, V.A. Shabashov, E.G. Volkova, A.E. Zamatovskii, A.V. Litvinov, V.V. Sagaradze, A.L. Osintseva. *Phys. Met. Metallogr.*, **118** (1), 52 (2017).  
DOI: 10.1134/S0031918X17010045
- [28] V.A. Shabashov, A.V. Makarov, K.A. Kozlov, V.V. Sagaradze, A.E. Zamatovskii, E.G. Volkova, S.N. Luchko. *Phys. Met. Metallogr.*, **119** (2), 180 (2018).  
DOI: 10.1134/S0031918X18020096
- [29] G.K. Williamson, W.H. Hall. *Acta Metall.*, **1**, 22 (1953).  
DOI: 10.1016/0001-6160(53)90006-6
- [30] N. Narkevich, Ye. Deryugin, Yu. Mironov. *Metals*, **11**, 710 (2021). DOI: 10.3390/met11050710
- [31] N.A. Narkevich, I.V. Vlasov, M.N. Volochev, Yu.F. Gomorova, Y.P. Mironov, S.V. Panin, F. Berto, P.V. Maksimov, E.E. Deryugin. *Metals*, **13**, 95 (2023).  
DOI: 10.3390/met13010095
- [32] S. Martin, S. Wolf, U. Martin, L. Krüger, D. Rafaja. *Metall. Mater. Trans. A*, **47**, 49 (2016).  
DOI: 10.1007/s11661-014-2684-4
- [33] Ya.B. Friedman. *Mekhanicheskie ispytaniya. Konstrukcionnaya prochnost'* (in two volumes) (*Mashinostroenie, M.*, 1974), vol. 2 (in Russian).
- [34] G.V. Klevtsov, L.R. Botvina, N.A. Klevtsova, L.V. Limar. *Fraktodiagnostika razrusheniya metallicheskih materialov i konstruktsiy* (*MISiS, M.*, 2007) (in Russian).
- [35] G.V. Klevtsov, R.Z. Valiev, N.A. Klevtsova, M.R. Kashapov, M.V. Fesenyuk, A.V. Ganeev, A.G. Raab. *Fundamental'nye issledovaniya*, **12** (2), 345 (2011) (in Russian).

*Translated by A.Akhtyamov*